Journal of Parkinson's Disease 14 (2024) 81–94
DOI 10.3233/JPD-230129
IOS Press

Research Report

Alpha-Synuclein Pre-Formed Fibrils Injected into Prefrontal Cortex Primarily Spread to Cortical and Subcortical Structures

Matthew A. Weber[a], Gemma Kerr[a], Ramasamy Thangavel[a], Mackenzie M. Conlon[b], Serena B. Gumusoglu[c,d], Kalpana Gupta[a], Hisham A. Abdelmotilib[a], Oday Halhouli[a], Qiang Zhang[a], Joel C. Geerling[a,d], Nandakumar S. Narayanan[a,d] and Georgina M. Aldridge[a,d,*]
[a]*Department of Neurology, Carver College of Medicine, University of Iowa, Iowa City, IA, USA*
[b]*Medical Scientist Training Program, Carver College of Medicine, University of Iowa, Iowa City, IA, USA*
[c]*Department of Obstetrics and Gynecology, Carver College of Medicine, University of Iowa, Iowa City, IA, USA*
[d]*Iowa Neuroscience Institute, University of Iowa, Iowa City, IA, USA*

Accepted 13 November 2023
Pre-press 30 December 2023
Published 23 January 2024

Abstract.
Background: Parkinson's disease dementia (PDD) and dementia with Lewy bodies (DLB) are characterized by diffuse spread of alpha-synuclein (α-syn) throughout the brain. Patients with PDD and DLB have a neuropsychological pattern of deficits that include executive dysfunction, such as abnormalities in planning, timing, working memory, and behavioral flexibility. The prefrontal cortex (PFC) plays a major role in normal executive function and often develops α-syn aggregates in DLB and PDD.
Objective: To investigate the long-term behavioral and cognitive consequences of α-syn pathology in the cortex and characterize pathological spread of α-syn.
Methods: We injected human α-syn pre-formed fibrils into the PFC of wild-type male mice. We then assessed the behavioral and cognitive effects between 12- and 21-months post-injection and characterized the spread of pathological α-syn in cortical, subcortical, and brainstem regions.
Results: We report that PFC PFFs: 1) induced α-syn aggregation in multiple cortical and subcortical regions with sparse aggregation in midbrain and brainstem nuclei; 2) did not affect interval timing or spatial learning acquisition but did mildly alter behavioral flexibility as measured by intraday reversal learning; and 3) increased open field exploration.
Conclusions: This model of cortical-dominant pathology aids in our understanding of how local α-syn aggregation might impact some symptoms in PDD and DLB.

Keywords: Prefrontal cortex, alpha-synuclein, Parkinson's disease, behavioral flexibility, exploratory behavior

*Correspondence to: Georgina M. Aldridge, MD, PhD, 169 Newton Road, Pappajohn Biomedical Discovery Building– 5334, University of Iowa, Iowa City, IA 52242, USA. Tel.: +1 319 384 1635; E-mail: georgina-aldridge@uiowa.edu.

INTRODUCTION

Patients with brainstem alpha-synuclein (α-syn) pathology have motor characteristics of Parkinson's disease (PD), including rigidity, bradykinesia, and tremor [1]. However, patients with PD dementia (PDD) and dementia with Lewy bodies (DLB), collectively termed Lewy body dementias (LBD), have diffuse spread of α-syn throughout the brain, including cortical regions [2, 3]. These patients often suffer from severe symptoms, including executive and working memory deficits, fluctuations in arousal and attention, hallucinations and psychosis, and increased risk for delirium [3–6]. It is not known whether the spread of α-syn to the cortex causes the symptoms of dementia, such as impaired cognition, or whether cortical α-syn simply reflects a more general process of spread and severity that does not directly affect cortical and cognitive function. To date, there are very few effective therapies approved to manage the debilitating cognitive symptoms of dementia [7, 8]; thus, it is critical that we understand the etiological factors of the diverse symptoms seen in LBD.

To investigate the impact of cortical-predominant pathology, we induced α-syn aggregation using human pre-formed fibrils (PFFs) injected in the prefrontal cortex (PFC) of wild-type mice, which can induce aggregation of native α-syn that resembles the pathology described in PDD and DLB [9–12]. Prior literature has extensively studied both mouse and human α-syn injected in the rodent striatum, the predominant model currently used primarily due to its unique ability to induce cell loss in the substantia nigra [11, 13]. A few studies have used varying injection locations, including duodenal, pedunculopontine nucleus, nucleus accumbens, olfactory bulb, and others [14–20]. These studies have offered mixed results regarding behavioral deficits and often restrict analyses to 6–7 months post injection (mpi). Furthermore, only a few studies have investigated PFC PFF injections [21–23]. A prior report from our group found no changes in interval timing behavior, novel object recognition, or open field behavior in mice that had a combined viral overexpression/PFF expression strategy and aged to 15 months (6 mpi) [23]. Cohorts of mice from this study and from our prior report were injected with PFFs in the PFC at approximately the same time. We hypothesized that PFC PFFs alone, in the context of advancing age and greater pathological burden, would negatively affect both interval timing and other behaviors. Thus, in this study, we investigated the effect of PFC PFFs on cortical, subcortical, midbrain, and brainstem α-syn pathology in mice aged up to 2 years (21 mpi) with a broader range of behavioral assays and challenges.

We report three main results: 1) PFFs injected in the PFC caused a consistent pattern of moderate-to-severe pathological α-syn aggregation in cortical and subcortical regions with sparse aggregation in midbrain and brainstem nuclei; 2) cognitive behaviors were mildly affected in mice injected with PFFs in the PFC, with no change in interval timing or spatial working memory acquisition, but a small, consistent alteration in behavioral flexibility as measured by intraday reversal learning; and 3) mice with cortical PFFs showed greater exploration of the center of an open field, without a change in total distance traveled. Together, these data suggest that aggregation of α-syn in cortical regions impacts specific behaviors in the absence of midbrain/brainstem inclusion. These results provide insight into cortical synucleinopathy, which is relevant for LBD and other synucleinopathies.

MATERIALS AND METHODS

Mice

All experimental procedures were performed in accordance with relevant guidelines by the University of Iowa Institutional Animal Care and Use Committee (IACUC). A total of 16 wild-type male C57BL/6 mice were received from Jackson Labs (Bar Harbor, ME) at approximately 8–10 weeks of age and acclimated to the animal holding facility for 1–2 weeks. All mice were communally housed on a 12 h light/dark cycle with *ad lib* access to standard laboratory chow and water, except as noted. The timeline of experiments is shown in Fig. 1.

Monomer and fibril preparation

Prepared monomeric alpha synuclein and human PFFs were a contribution from Dr. Andrew West and prepared according to previously used protocols [23, 24]. Briefly, fibrils were sonicated with a 1/8 inch probe tip at 30% power (Fisher Scientific Sonic Dismembrator FB120110) in 15 s intervals, aliquoted, and frozen at –80°C by the donating lab before being shipped. Monomers and PFFs were shipped on dry ice and stored at –80°C, thawed and kept on ice immediately prior to surgical procedures, and resuspended prior to each stereotaxic injection. Potentially

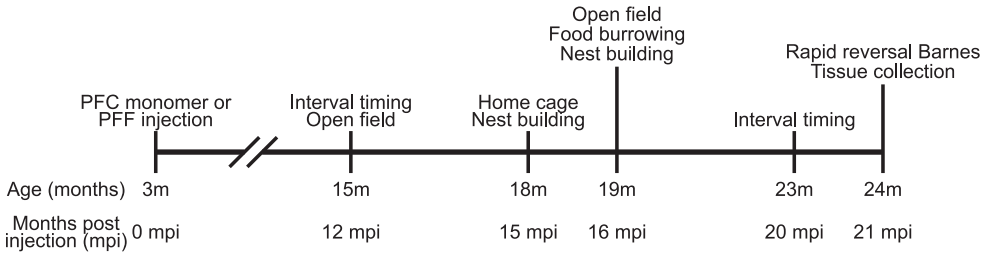

Fig. 1. Experimental timeline.

contaminated surfaces were then thoroughly cleaned with 10% bleach.

Surgical procedures

Mice were anesthetized under 4.0% isoflurane and surgical levels of isoflurane (1.5–3.0%) were sustained for the duration of the surgery (SomnoSuite, Kent Scientific, Torrington, CT, USA). Analgesic (carprofen) and local anesthetic (bupivacaine) were administered prior to the start of surgery. An incision was made along midline and bilateral burr holes drilled above the PFC, and a Hamilton syringe was lowered to the target coordinates (AP + 1.8, ML ± 0.5, DV-1.5). Mice were assigned to bilateral microinjections of either 2 μL monomers ($n = 8$) or 2 μL PFFs ($n = 8$). Monomeric controls or PFFs were infused over 20 min (0.1 μl/min; Legato 130 Syringe Pump, kd Scientific, Holliston, MA, USA), with a 5 min wait period before removing the needle. The incision was then sutured, and mice were moved to a clean cage with *ad lib* access to food and water. Behavioral testing began approximately 12 months later (Fig. 1).

Interval timing switch task

All mice were trained to perform an interval timing switch task (Fig. 4A) described in detail previously [25–28]. Interval timing behavior was assessed on two occasions: 1) 12 mpi; 2) 20 mpi. Briefly, food-restricted mice are trained in standard operant chambers (MedAssociates, St. Albans, VT) equipped with two nosepoke response ports (left and right) flanking a reward hopper and another nosepoke response port on the backwall. Either the left or right nosepoke was designated for short trials and the contralateral nosepoke for long trials (counterbalanced across mice and experimental groups). Trials are initiated by a response at the back nosepoke, which generated identical cues for both the left and right nosepokes. In short trials, mice receive a reward for the first response after 6 s. In long trials, mice receive a reward for the first response after 18 s. Because cues are identical for both short and long trials, the optimal strategy is to start responding at the short nosepoke and switch to the other nosepoke to receive a reward if enough time passed without reward.

Rapid reversal barnes maze

A modified Barnes maze (Fig. 4F) was used to evaluate spatial learning acquisition and behavioral flexibility adapted from established protocols [29, 30], with the following notable exceptions: 1) the spatial target was changed every day to a new random location and every 4 trials to an opposite location in order to assess rapid acquisition of a spatial target (first 4 trials) and intraday reversal learning (last 4 trials); 2) to minimize the use of olfactory cues, every hole was equipped with its own 3D printed escape box "shuttle" such that no shuttle was ever re-used during a session, and the maze itself was also rotated. A plastic grate made of identical material prevented entry to incorrect shuttles; 3) following a correct response (entry), the shuttle was connected by tunnel with the home cage as a potent reward, during a 3 minute inter-trial interval; 4) a 40-hole circular Barnes maze apparatus was used in which only 10 holes were available. Total distance traveled was captured with overhead cameras and analyzed using ANY-Maze 7.14d (Stoelting, Wood Dale, IL).

Open field

Open field activity was used to assess exploration and activity levels on two occasions (12 and 16 mpi), using methods described previously [31, 32]. On each occasion, mice were habituated to behavior rooms for at least 30 minutes prior to testing. Mice were placed

in the center of an empty open field arena (40 cm × 40 cm × 30 cm) and allowed to explore uninterrupted for 10 min. Mice were returned to their home cage immediately, and the open field arenas were thoroughly cleaned with 70% ethanol and allowed to air dry between trials. Rescue disinfectant (0.5% hydrogen peroxide) was used between cohorts. Total distance traveled and thigmotaxis (distance traveled outside a 25.5 × 25.5 cm central square divided by total distance traveled) were analyzed using ANY-Maze 7.14d.

Home cage activity

Home cage activity was assessed in parallel with nest building and food burying (described below) at 15 mpi. Overhead cameras captured morning and nighttime activity using an infrared camera. ANY-Maze 7.14d software was then used to quantify periods of activity and rest over a 1 h period during the morning (∼6–7 am) and night (∼2–3 am). Midday activity could not be quantified due to unexpected interference with lighting through cage bars. Periods of immobility were defined as periods 40 s or longer during which ANY-Maze did not detect movement. Percent immobile was then defined as the number of seconds the mouse spent immobile compared with total seconds tracked. Bout length was based on prior published data using electroencephalography suggesting that periods of immobility greater than 40 s are likely to be sleep bouts [33].

Nesting

Nest building was used to approximate general health and welfare, using slightly modified methods described previously [34]. Nesting behavior for each mouse was assessed on two occasions (15 and 16 mpi). At 15 mpi, three different materials (shredded paper, paper twist, and pressed cotton square) were provided on separate days. At 16 mpi, only the paper nest building material was provided. Photographs were taken of each nest and scored by blinded observers on a scale of 1–5 according to previous literature [34, 35].

Food burying

Food burying was assessed in parallel with nest building at 16 mpi. Pre-weighed food was provided in a glass jar equipped with a PLA 3D printed cone-shaped hopper to prevent mice from nesting in the jar. The jar was weighed the following day to calculate food buried or eaten.

Histology

Mice were anesthetized with ketamine (100 mg/kg IP) and xylazine (10 mg/kg IP) and transcardially perfused with phosphate-buffered saline (PBS) and 4% paraformaldehyde (PFA). Brains were fixed in 4% PFA overnight and immersed in 30% sucrose for approximately 48 hours. Brains were then serially sliced into 40 μm coronal sections using a cryostat (Leica Biosystems, Deer Park, IL). Brain sections were blocked for 1 h in 2% normal goat serum (NGS) in PBST (0.3% Triton X-100 in 1x PBS) and then incubated for approximately 20 h at 4°C in either rabbit anti-α-synuclein (α-syn) phosphorylated serine 129 (P-S129; Abcam #EP1536Y, Cambridge, United Kingdom) diluted to 1 : 1000 in blocking solution or rabbit anti-tyrosine hydroxylase (TH; Millipore #AB152, Burlington, MA) diluted to 1 : 1000 in blocking solution. Sections were then washed in PBS three times and incubated overnight at 4°C in goat anti-rabbit IgG (*H* + L) Alexa Fluor 647 secondary antibody (Invitrogen #A11036, Waltham, MA) diluted to 1 : 1000 in blocking. Sections were washed three more times. To stain for nissl, sections were washed in PBST for 10 min and two additional 5 min washes in PBS. Sections were incubated in NeuroTrace™ 435/455 (Thermo Fisher Scientific Inc. #N21479, Waltham, MA) diluted 1 : 300 in PBS for 20 min at room temperature and then washed in PBST for 10 min and twice in PBS for 5 min each. After one more wash at room temperature for 2 h, sections were mounted with ProLong Diamond Antifade Mountant (Invitrogen #P36961) on Super frost microscope slides (Fisher Scientific).

All sections were imaged using VS-ASW-S6 imaging software (Olympus, Center Valley, PA) and an Olympus Slide Scanner (Olympus VS120) with a 20x objective. To characterize pathological spread of α-syn, we semi-quantitively graded the degree of P-S129 inclusions in multiple regions of interest (ROI; see Fig. 2 for complete list) referenced from Franklin and Paxinos (2008) [36]. The α-syn pathology was graded using the rubric images from previously published literature [37]. We chose to use a semi-quantitative analysis of pathological α-syn burden rather than quantifying α-syn densities as our strategy of PFC seeded PFFs did not result in robust behavioral changes, which is described in more detail below. Briefly, pathology was assigned on a scale of 0–4

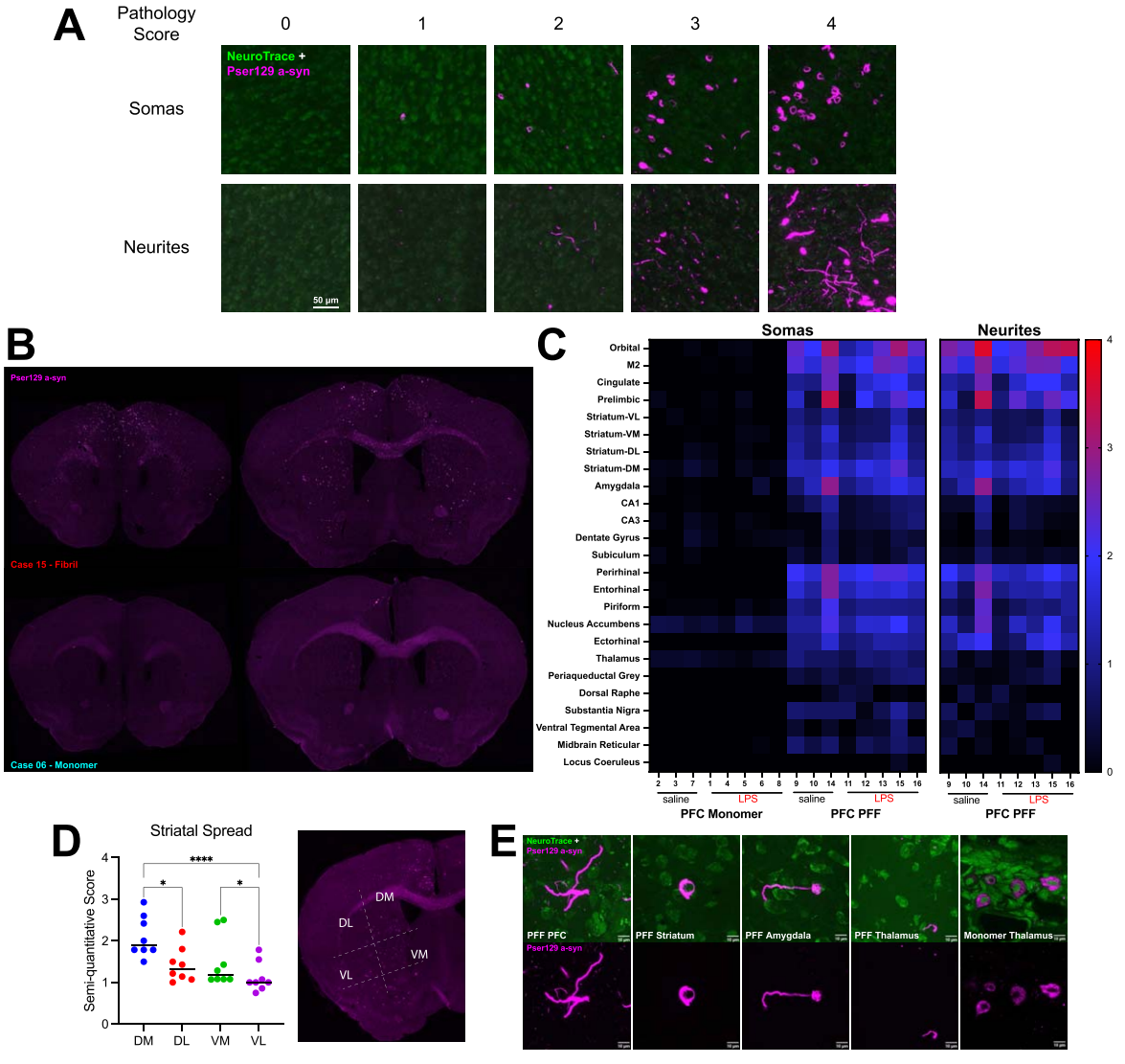

Fig. 2. Evaluation of pathology in monomer control and pre-formed fibril (PFF) injected mice. A) Example images α-synuclein (α-syn) positive somas (top row) and neurites (bottom row) used to score pathology as described in the methods. B) Top: representative images from the prefrontal cortex and striatum in one mouse treated with PFFs. Bottom: representative images from the prefrontal cortex and striatum in one monomer control mouse. C) Semi-quantitative scores of α-syn positive somas (left panel) and neurites (right panel) of 25 brain regions, with each column representing an individual mouse, averaged over the entire rostral-caudal extent for each brain region examined. Neurites for monomer mice are not displayed as there were zero p-α-syn positive neurites in any region of any mouse. Note that mice are separated by saline and lipopolysaccharide treatment described in more detail in the Supplementary Material. D) Left panel: averaged semi-quantitative score of pathological α-syn within subregions of the striatum restricted to 0–1.7 mm bregma. Subregions of the striatum (DM, dorsomedial; DL, dorsolateral; VM, ventromedial; VL, ventrolateral) were referenced from previous literature [68]. Horizontal bars indicate group medians. * $p < 0.05$, **** $p < 0.0001$. Right panel: representative image of striatal subregions from one mouse treated with PFFs. E) Confocal images showing examples of fibrillar pathology in multiple brain regions from PFF injected mice (panels 1–4). Monomer mice showed rare p-α-syn positive puncta, without clear fibrillar morphology (panel 5). No fibrillar or neurite pathology was found in monomer mice using confocal microscopy.

separately for neurites and somas, with the following general guidelines, in addition to published rubric, to assist and calibrate blinded grading; 0: no soma or neurite P-S129 positive staining; 1) sparse/light soma or neurite staining (1–3 somas or neurites per 750 μm square area within ROI); 2) mild burden (4 or more somas or neurites per 750 μm, with definitive areas showing no P-S129 staining); 3) dense burden (> 10 soma or neurites per 250 μm); 4) heavy burden (> 20 somas or neurites per 250 μm). Repre-

sentative images for soma and neurite pathological scores are shown in Fig. 2A, and differences between a single monomer-treated control mouse and a single PFF-treated mouse are shown in Fig. 2B. Representative images across the rostral-caudal aspect of the brain (approximately + 3.5 – –6 mm AP to bregma) in two monomer-treated control mice and two PFF mice are shown in Supplementary Figure 3. For every brain, one out of every six 40 μm sections were graded for α-syn inclusion. Results from brain regions that spanned multiple sections were averaged across sections and hemispheres, even if some sections contained no pathology.

To quantify potential neuron loss in the prefrontal cortex (prelimbic, cingulate, and medial M2), we determined neuronal densities via stereological estimates of NeuroTrace (Stereo-investigator, Microbrightfield, Colchester, Vermont; Axiocam, Zeiss, Oberkochen, Germany), using methods described previously [38–41]. We quantified density within three-dimensional counting frames measuring 100 × 100 × 10 μm. These frames were systematically positioned across a randomized grid of 500 × 500 μm. Boundaries of the prefrontal cortex were determined using Franklin and Paxinos (2008) [36]. Coronal sections from 1.18–2.46 mm anterior of bregma were selected and an ∼1 mm mediolateral area (encompassing prelimbic, cingulate, and medial M2) was analyzed across 3–4 sections for each animal from the monomer control and PFF groups. Cell quantification was accomplished by employing an optical fractionator, adhering to unbiased counting principles of stereology as outlined previously [42]. This approach uses randomly positioned counting frames and ensures equilibrium between the exclusion and inclusion boundaries of these frames. Density was computed by dividing cell count by the measured volume determined by Stereo-investigator.

Statistics

Sample sizes were chosen based on published datasets [27, 28] in which a 25% change was detected in interval timing behavior. Based on this prior work, we anticipated an effect size of 1.86 with 8 mice per group (PFC monomers vs. PFC PFFs) if a significant change in interval timing was observed. All data was analyzed using custom written MATLAB routines and Graphpad Prism. Pathology scores (ordinal) were analyzed using Friedman Rank Sum test. Tyrosine hydroxylase values (quantitative intensity) were analyzed using repeated-measures ANOVA. Behavioral tasks and PFC densitometry were analyzed using separate unpaired *t*-tests or repeated measures ANOVA. Separate nest building scores (ordinal) were analyzed using separate Mann-Whitney *U* tests. Our statistical approach was reviewed by the Biostatistics Epidemiology and Research Design Core in the Institute for Clinical and Translational Sciences at the University of Iowa.

RESULTS

PFFs injected in the medial prefrontal cortex led to cortical and subcortical synuclein aggregation

Injections of PFFs in the PFC led to α-syn aggregation in the injected cortical area as well as several downstream regions. We found clear and dense pathological spread of α-syn in orbitofrontal, secondary motor M2, perirhinal, entorhinal, piriform, nucleus accumbens, amygdala, and thalamus (Fig. 2C). Subregions of the striatum were differentially affected by PFFs injected in the PFC (Fig. 2D). A Friedman test was conducted and there was a statistically significant difference in α-syn aggregation between subregions of the striatum ($\chi^2(3) = 22.2$, $p < 0.0001$). *Post*-hoc analyses using Dunn's multiple comparisons test revealed significant differences between dorsomedial and dorsolateral striatum ($p = 0.04$), dorsomedial and ventrolateral striatum ($p < 0.0001$), and ventromedial and ventrolateral ($p = 0.04$). Unlike other subcortical regions, subregions of the hippocampus were considerably less dense, and similar sparse-to-absent pathological α-syn aggregation was observed in regions of the midbrain and brainstem.

We also quantified tyrosine hydroxylase positive (TH+) fluorescence levels in the PFC, striatum, ventral tegmental area, and substantia nigra (Fig. 3A), similar to prior methods established in the lab [28]. As expected, there was a statistically significant difference in TH+ fluorescence levels between regions (Fig. 3A; two-way repeated-measures ANOVA; main effect of region ($F_{(1.105, 15.47)} = 122.9$; $p < 0.0001$), but we found no significant change in TH+ fluorescent levels in PFF-injected mice compared with controls in any of the four regions (main effect of treatment ($F_{(1,14)} = 0.2078$; $p = 0.66$). Further, we did not find any differences in markers for astrocyte (GFAP) or microglia (IBA-1) activation (Supplementary Figure 1H). Similar to previous literature [41], there was no significant difference in cell density (as stained with NeuroTrace) in the prefrontal cortex of PFF-injected mice compared to monomer controls

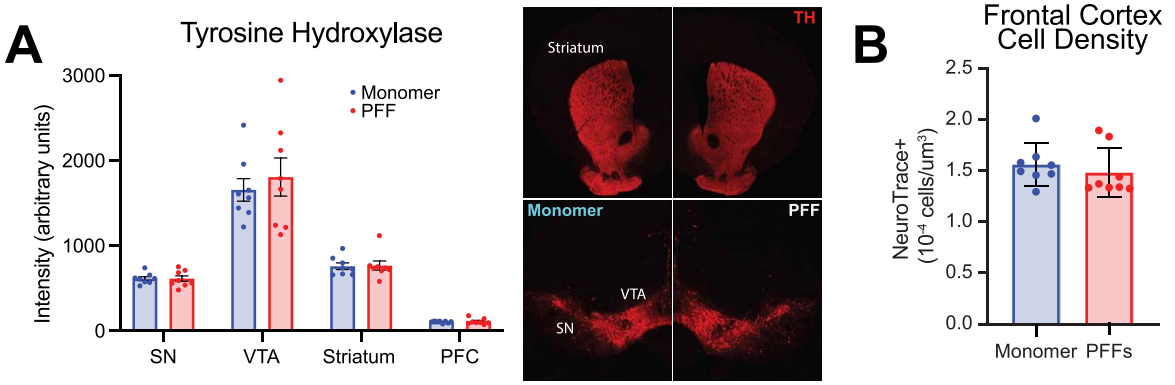

Fig. 3. Evaluation of tyrosine hydroxylase (TH) and prefrontal cortex densitometry in monomer control and pre-formed fibril (PFF) injected mice. A) Left panel: TH intensity (arbitrary units) from 4 different brain regions in monomer and PFF treated mice: substantia nigra (SN), ventral tegmental area (VTA), striatum, and prefrontal cortex (PFC). Right panel: representative images of TH in the SN, VTA, and striatum from a monomer treated mouse (left) and PFF treated mouse (right). B) PFC neuron densitometry. PFF treated mice did not differ from monomer controls ($p = 0.5$). All data from 8 monomer (blue) and 8 PFF (red) mice. All data are expressed as mean ± SEM, and each dot represents a single mouse.

(Fig. 2B; unpaired *t*-test; $t(14) = 0.6954$; $p = 0.50$). The Gundersen Coefficient of Error, which is used to measure error in unbiased stereology [43], was < 0.07 for all mice, indicating sampling design contributed to less than 7% of the total variability of the measures.

PFFs injected in the medial prefrontal cortex does not induce mortality

Surgical procedures and injection of monomers or PFFs in the PFC did not induce any mortality. All mice survived until 19 mpi at which point two monomer-treated mice were sacrificed due to age-related health concerns per the University of Iowa Office of Animal Resources guidelines. At 20 mpi, two PFF-treated mice were also sacrificed due to age-related concerns and one monomer-treated mouse was found dead. Finally, all remaining mice were sacrificed at the experimental endpoint of 21 mpi.

PFFs injected in the medial prefrontal cortex cause mild changes in behavioral flexibility but do not change interval timing performance

Interval timing requires mice to estimate an interval of several seconds and requires working memory for temporal rules as well as attention to the passage of time. Our prior work showed no deficits in interval timing using a fixed-interval timing task at 15 months of age (6 mpi of PFFs) [23]. Here, we sought to investigate interval timing performance in mice at 12 + mpi, using an interval timing switch task that enables us to track mean temporal estimates as well as the variability of temporal estimates. We found that at 12 mpi, mice injected with PFFs showed no difference in mean switch times (shifting early or late as an estimate of timing accuracy; Fig. 4B; unpaired *t*-test; $t(13) = 0.66$; $p = 0.52$) and no difference in switch time coefficient of variance (estimate of timing precision; Fig. 4C; unpaired *t*-test; $t(13) = 1.05$; $p = 0.31$). One PFF injected mouse was excluded because no trials initiated or rewards obtained, likely due to a lack of motivation to perform the task. We repeated interval timing switch task training at 20 mpi. Because two monomer-treated mice were sacrificed at 19 mpi due to age-related health concerns, this round of interval timing training included six monomer and eight PFF mice. Similar to interval timing at 12 mpi, we found no difference in mean switch times (Fig. 4D; unpaired *t*-test; $t(12) = 0.29$; $p = 0.78$) or the coefficient of variance of switch times (Fig. 4E; unpaired *t*-test; $t(12) = 1.20$; $p = 0.25$). We found no difference in the proportion of rewarded trials at either timepoint (Supplementary Figure 2A, B). Together, these results suggest that PFC PFFs do not affect interval timing behavior even at 20 mpi.

After interval timing training, one mouse treated with monomers was found dead and two mice treated with PFFs were sacrificed due to age-related health concerns. Therefore, five monomer and six PFF mice remained. To test learning and behavioral flexibility, all remaining mice were tested using a rapid reversal Barnes maze at 21 mpi. PFF mice showed an altered pattern of behavior flexibility,

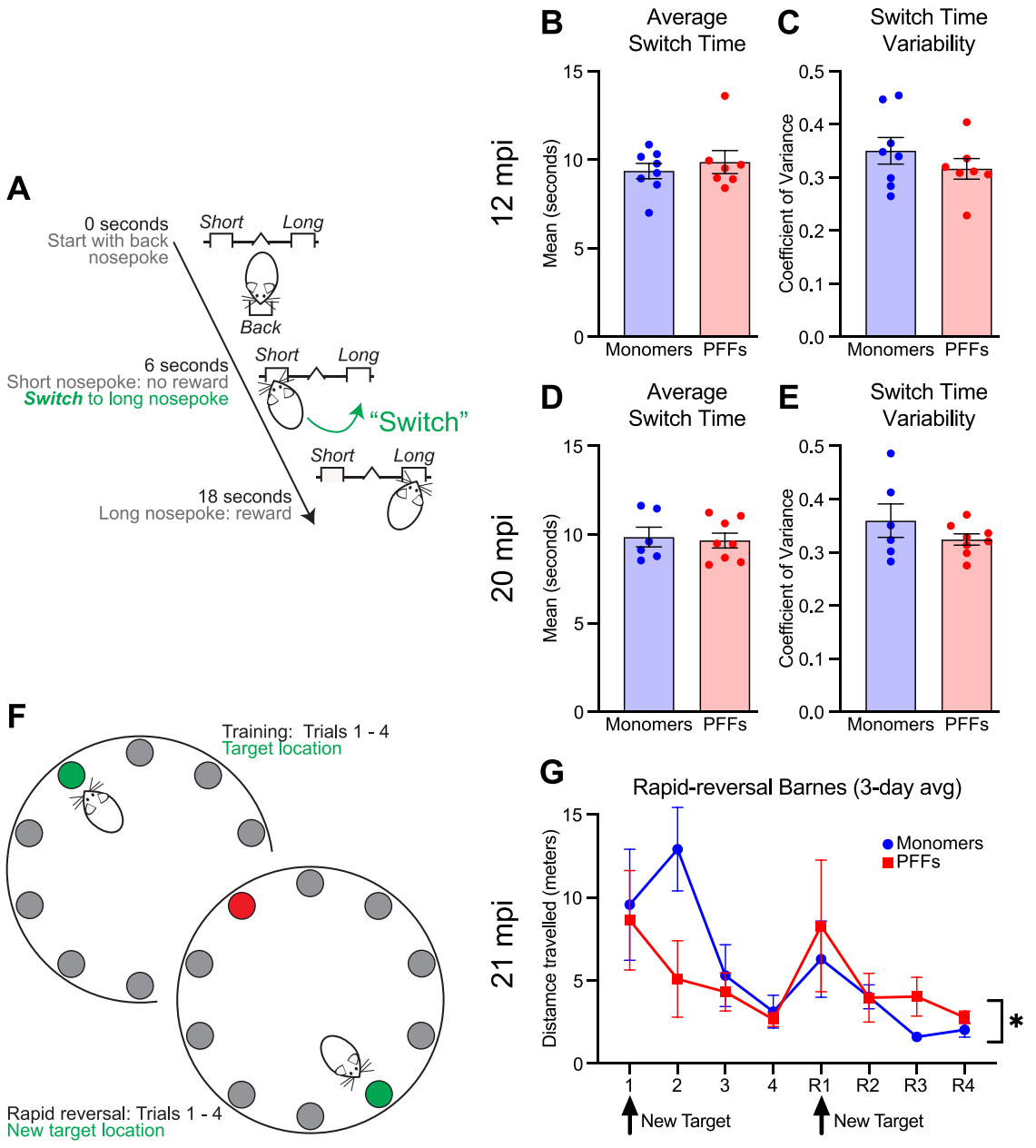

Fig. 4. Interval timing and reversal learning in monomer control and PFC PFF mice. A) Diagram for the interval timing switch task outlining optimal performance during long trials. B) Mean switch time and C) switch time coefficient of variance during the interval timing task at 12 mpi. Data from 8 monomer (blue) and 7 PFF (red) mice. D) Mean switch time and E) switch time coefficient of variance during the interval timing task. Data from 6 monomer (blue) and 8 PFF (red) mice. Each dot represents a single mouse. F) Diagram for the rapid reversal Barnes maze. G) Average total distance travelled averaged across three-days. There was a main effect of trial and trial×treatment interaction. * $p < 0.05$, but *post*-hoc testing at specific trials did not survive multiple comparisons. Data from 5 monomer (blue) and 6 PFF (red) mice. Data are expressed as mean ± SEM.

with PFF mice learning quickly during the initial trials, but then travelling a greater distance to reach the target compared with control mice during the reversal phase (Fig. 4G; two-way repeated-measures ANOVA; main effect of trial ($F_{(2.145,19.31)} = 6.71$; $p = 0.005$) and trial×treatment interaction ($F_{(7,63)}$

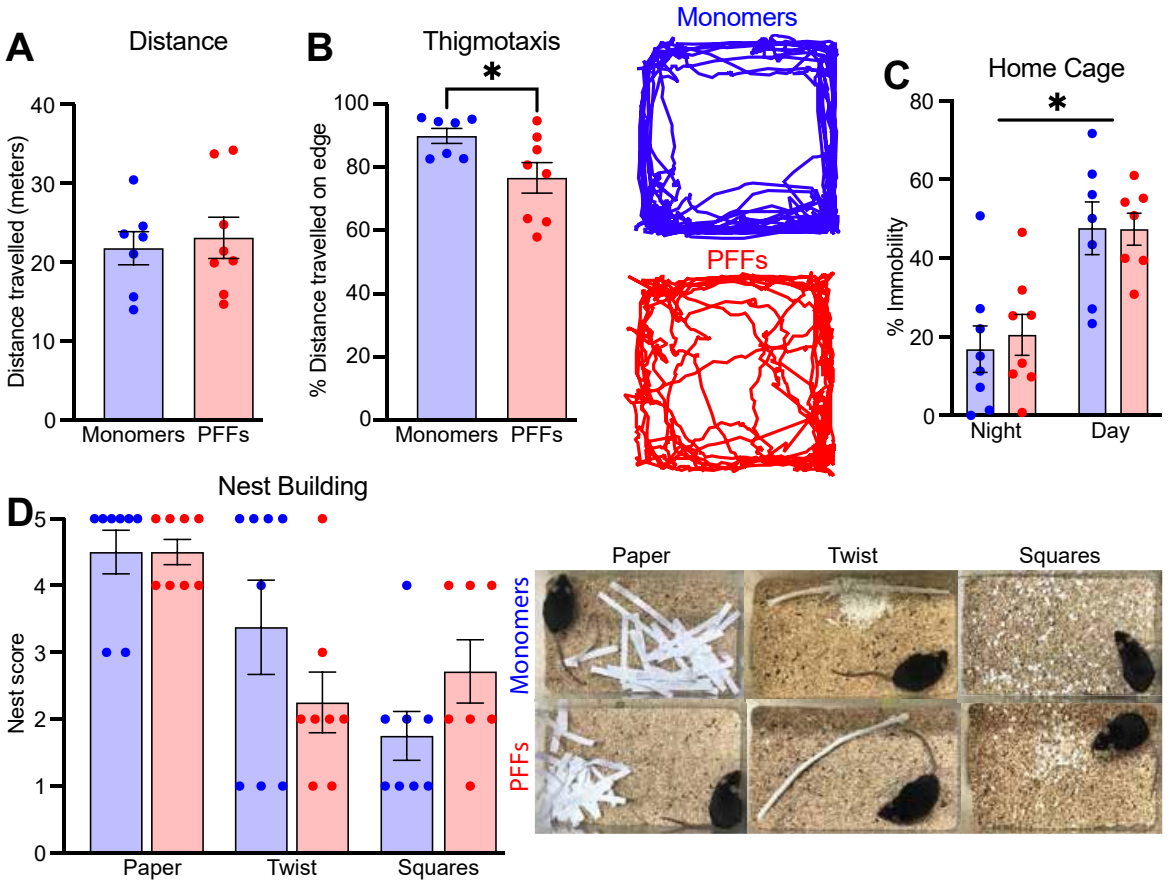

Fig. 5. A) Distance travelled and B) thigmotaxis during the open field test. The right panel is an example trace from one monomer and one PFF mouse during the open field assay. C) Percent immobility time between ~2–3 am (night) and ~6–7 am (morning). D) Nest building score for three different materials (shredded paper, cotton twist, and precut cotton squares) with representative images from each material shown in the right panel. Data from 8 monomer (blue) and 7–8 PFF (red) mice. All data are expressed as mean ± SEM, and each dot represents a single mouse. *$p < 0.05$.

$= 2.17$; $p = 0.049$); *post*-hoc analyses revealed no significant differences when corrected for multiple-comparisons). A similar pattern of behavior during the reversal phase, although not statistically different, was observed during a single day rapid reversal Barnes protocol at 17 mpi (Supplementary Figure 2G).

PFFs injected in the medial prefrontal cortex reduces thigmotaxis

We assessed exploration and activity levels in the open field. At 12 mpi, mice injected with PFFs in the PFC did not differ from monomer controls in distance traveled (meters) over the 10 minute test (Fig. 5A; unpaired *t*-tests; $t(13) = 0.35$; $p = 0.73$), but did display reduced thigmotaxis, showing more exploration of the center of the arena (Fig. 5B; unpaired *t*-tests; $t(13) = 2.49$; $p = 0.03$). These results may suggest greater exploration or reduced anxiety-like behavior in PFC PFF injected mice.

PFFs injected in the medial prefrontal cortex does not alter home cage activity or nest building (15 mpi)

To assess general health and welfare as well as naturalistic behaviors, we used assays to examine home cage activity and nest building. At 15 mpi, mice injected with PFFs in the PFC did not differ on amount of home cage activity during either the light or dark cycle (Fig. 5C; mixed-effects two-way ANOVA; main effect of treatment $F_{(1,14)} = 0.04$; $p = 0.84$), but there was a significant main effect of time of day ($F_{(1,12)} = 50.45$; $p < 0.0001$). At the same time-point, there were no differences in nest building score across

three different types of material (Fig. 5D; Mann-Whitney U; paper $p = 0.61$; twist $p = 0.42$; squares $p = 0.18$). Altogether, these data suggest that PFC PFFs do not reduce naturalistic innate behaviors or overall well-being.

DISCUSSION

We tested the effects of PFC PFFs in aged mice on multiple behavioral assays and then evaluated spread of α-syn aggregation in cortical, subcortical, and brainstem regions. First, we found that PFC PFF injection triggered widespread cortical and subcortical α-syn aggregation, without significant spread to brainstem regions. Further, we did not find a difference in PFC cell density, which is similar to prior work [41], nor a difference in TH positive fluorescence levels in any of the regions examined. Together, these findings allow us to evaluate the behavioral impact of α-syn limited to these regions. Second, and in line with our prior work, we found no reliable deficits in interval timing, but we did find mild alterations in reversal learning. Third, we also found changes in exploration without changes in distance travelled in the open field assay. Taken together, these data contribute to understanding potential consequences of cortical α-syn, which is important for efforts investigating the role of this pathological finding in synucleinopathies such as PDD and DLB.

The rodent PFC is a highly connected brain region, sending projections to multiple cortical, subcortical, midbrain, and brainstem nuclei [44, 45]. Our prior work suggested that human PFFs injected into PFC cause a consistent but spatially limited pattern of α-syn pathology including PFC, temporal cortex, and striatum. The consequences of α-syn outside of the brainstem, as occurs in PDD and DLB, are still relatively unknown. Using the model of cortically-injected PFFs helps tease out the consequences of cortical/subcortical α-syn pathology in the absence of dramatic loss of neurons in brainstem regions. Using semi-quantitative analysis of 25 brain regions, we demonstrate dense pathological spread of α-syn in multiple cortical regions such as the orbitofrontal, secondary motor M2, perirhinal, entorhinal, and piriform. A consistent pattern of α-syn was also observed in subcortical regions, including the striatum, nucleus accumbens, amygdala, and thalamus. We note that there is differential aggregation of α-syn in subregions of the striatum, matching the connectivity of our prefrontal injection site and in line with prior work from Gabbott and colleagues (2005) [46]. We targeted the dorsal prelimbic and anterior cingulate subregions of the PFC, which contain a greater number of neurons that project to the dorsal striatum compared to the ventral prelimbic and infralimbic subregions of the PFC that contain more ventral striatal projecting neurons [46]. We also note that, unlike other subcortical regions, the subregions of the hippocampus were relatively spared from α-syn aggregation. This finding was again in line with prior literature suggesting that cortical input to the hippocampus passes through the perirhinal and entorhinal cortices first [47], two areas that show dense α-syn deposition here. While there was clear α-syn in cortical and subcortical regions, we found little or no α-syn pathology in midbrain and brainstem nuclei, including substantia nigra, locus coeruleus, and dorsal raphe. Together, these findings extend our prior work to show that the aggregation induced in cortical and subcortical regions by human PFFs injected into PFC are not cleared over the course of aging, as has been reported in some brain regions [48].

Notably, prior work from our group has shown that human PFFs injected in the PFC does not affect interval timing or open field behavior 6 mpi in mice aged 15 months [23]. By contrast, prior work has shown that people with PD display reliable deficits in interval timing [49–52] and that the PFC is crucial for interval timing behavior [49, 53, 54]. The data presented here, and our prior report demonstrate that PFC PFFs are not sufficient to affect interval timing. There are several hypotheses that could explain preserved interval timing in our PFF model: 1) midbrain dopaminergic cell loss, which is absent in this model, may be the main driver for interval timing deficits seen in PD and mouse models [28, 49]; 2) human PFFs may predominate in a PFC cell type that is not critical for interval timing; 3) seeding of human PFFs results in significantly less pathogenicity compared to mouse PFFs [55], which could result in the mild behavioral alterations observed here despite presence of pathology; 4) cortical cells may function even in the setting of α-syn aggregation, either because of the lack of neuronal cell loss observed here or through cellular or circuit-level compensation.

While α-syn aggregates were widespread and dense in cortical and subcortical regions, mice that received PFC PFF injections displayed only mild behavioral deficits. PFF mice did not display any difference in measures of interval timing, including variability of or mean switch times. This result is in line with prior work from our group [23] and

expands upon this work to show that PFC PFFs and the resulting α-syn aggregation is not sufficient to induce an interval timing deficit, even up to 20 mpi. However, we did find that PFF mice displayed reduced thigmotaxis at 12 mpi, with the same trend observed at both 16– and 21mpi (Supplementary Figure 1A, B and 1E, F), which was not observed in our prior report and may suggest a difference in explorative and anxiolytic behaviors in the open field as a result of PFC PFF injections. The role of the PFC in anxiety-like behavior is complex, with individual subregions exerting differential effects. For example, optogenetic stimulation of the ventromedial but not dorsomedial PFC reduces anxiety-like behaviors in the open field [56], whereas electrical stimulation of dorsal (prelimbic) PFC increases freezing behaviors in a fear-conditioning task [57]. Behavioral flexibility, including reversal learning, is also regulated by the prefrontal cortex [58], especially orbital frontal regions that showed significant pathology in our model. In this study, we found that PFF mice showed rapid spatial acquisition but required a longer search route to locate the target exit hole during the reversal phase of a daily spatial training Barnes maze task at 21 mpi, suggesting altered behavioral flexibility. As pathology was distributed throughout PFC in our model, circuit imbalance at multiple level could contribute to these behaviors. Further studies recording neuronal firing during behavior are necessary to understand whether loss of function, hyperexcitability, or cell-specific vulnerability contributes to behavioral changes.

This study has several limitations. First, our control animals received monomer injections, which has been shown previously to occasionally lead to mild and transient aggregation [59]. We did note some mild p-α-syn positive puncta and cells, but morphology was distinct, and may have been caused by aging alone. Fibrillar and "Lewy-neurite-like" structures were only seen in PFF injected mice, and this was confirmed by confocal microscopy. Similarly, monomer and PFF injections could potentially cause behavioral deficits through a non-aggregate mechanism that would not be observed without a vehicle-injected control group. Second, we did not investigate mouse PFFs seeded in the prefrontal cortex, which has been shown to induce greater α-syn pathology when seeded in the mouse striatum [55]. An important future direction would be to investigate whether cortically seeded mouse PFFs induce significant behavioral changes. Third, we did not investigate cell-type preference for human PFF-induced α-syn pathology, which could impact the response of the PFC. Furthermore, new evidence suggests human brain derived α-syn fibrils differ from PFFs and may lead to different cellular vulnerability; for example, recent publications have suggested PFFs also induce significant glial inclusions [60, 61], which are less common in DLB patients or mouse seeded with human-brain derived fibrils. Comparisons between brain derived vs. PFF models may help us understand disease heterogeneity. Fourth, we did not include a group of young mice to determine whether our lack of behavioral change was primarily due to age-related decline in cognitive function or interval timing, which has been observed previously [62, 63]. However, the interval timing behavior presented here is similar to previously published work from our group using healthy, young C57BL/6 mice [26, 64]. Fifth, our measures of interval timing and behavioral flexibility do not fully interrogate cognitive dysfunctions related to PDD and LBD and it is possible that other cognitive behaviors such as attention or impulse control were negatively affected by PFC PFF injections. Sixth, some behavioral experiments may be underpowered to detect subtle differences due to age-related loss, or < 25% change. This is particularly true for our exploratory LPS experiments in our Supplementary Material (Supplementary Figure 1), which are included to aid future investigations. Despite these limitations, due to careful pathological confirmation of each mouse in this two-year study, we believe these results inform future research and are important for understanding this model and considerations for testing other models to induce aggregation. Finally, this study was limited to male mice. Human males are more likely to be diagnosed with PD and DLB [65–67], and understanding potential differences in pathology due to sex is an essential goal of future research and fully powered studies of both sexes are needed.

In summary, our results describe widespread cortical and subcortical α-syn aggregation from PFC PFFs with mild behavioral alterations. The lack of brainstem involvement is notable and could provide insight into the brain networks that drive behavioral deficits in PD, PDD, and DLB.

ACKNOWLEDGMENTS

We thank Dr. Andrew West for generously providing the pre-formed fibrils and Travis Larson for assisting with behavioral experiments.

FUNDING

This work was supported by NIH R01s MH116043, NS120987 to NSN and NIH K08 NS109287, R01 NS129711, and the Iowa Neuroscience Institute to GMA. This work was also supported by NIH P20NS123151 to NSN and GMA. Additionally, HAWK-IDDRC (P50HD103556) and AHA award (#908921) supported SBG.

CONFLICT OF INTEREST

The authors have no conflict of interest to report.

DATA AVAILABILITY

All raw data are available at https://aldridge.lab.uiowa.edu/open-science.

All code is available at https://aldridge.lab.uiowa.edu/open-science.

SUPPLEMENTARY MATERIAL

The supplementary material is available in the electronic version of this article: https://dx.doi.org/10.3233/JPD-230129.

REFERENCES

[1] Braak H, Tredici KD, Rüb U, de Vos RAI, Jansen Steur ENH, Braak E (2003) Staging of brain pathology related to sporadic Parkinson's disease. *Neurobiol Aging* **24**, 197-211.

[2] Irwin DJ, Lee VM-Y, Trojanowski JQ (2013) Parkinson's disease dementia: Convergence of α-synuclein, tau and amyloid-β pathologies. *Nat Rev Neurosci* **14**, 626-636.

[3] McKeith IG, Boeve BF, Dickson DW, Halliday G, Taylor J-P, Weintraub D, Aarsland D, Galvin J, Attems J, Ballard CG, Bayston A, Beach TG, Blanc F, Bohnen N, Bonanni L, Bras J, Brundin P, Burn D, Chen-Plotkin A, Duda JE, El-Agnaf O, Feldman H, Ferman TJ, Ffytche D, Fujishiro H, Galasko D, Goldman JG, Gomperts SN, Graff-Radford NR, Honig LS, Iranzo A, Kantarci K, Kaufer D, Kukull W, Lee VMY, Leverenz JB, Lewis S, Lippa C, Lunde A, Masellis M, Masliah E, McLean P, Mollenhauer B, Montine TJ, Moreno E, Mori E, Murray M, O'Brien JT, Orimo S, Postuma RB, Ramaswamy S, Ross OA, Salmon DP, Singleton A, Taylor A, Thomas A, Tiraboschi P, Toledo JB, Trojanowski JQ, Tsuang D, Walker Z, Yamada M, Kosaka K (2017) Diagnosis and management of dementia with Lewy bodies: Fourth consensus report of the DLB Consortium. *Neurology* **89**, 88-100.

[4] Aldridge GM, Birnschein A, Denburg NL, Narayanan NS (2018) Parkinson's disease dementia and dementia with Lewy bodies have similar neuropsychological profiles. *Front Neurol* **9**, 123.

[5] FitzGerald JM, Perera G, Chang-Tave A, Price A, Rajkumar AP, Bhattarai M, O'Brien JT, Ballard C, Aarsland D, Stewart R, Mueller C (2019) The incidence of recorded delirium episodes before and after dementia diagnosis: Differences between dementia with Lewy bodies and Alzheimer's disease. *J Am Med Dir Assoc* **20**, 604-609.

[6] Lawson RA, McDonald C, Burn DJ (2019) Defining delirium in idiopathic Parkinson's disease: A systematic review. *Parkinsonism RelatDisord* **64**, 29-39.

[7] Halhouli O, Zhang Q, Aldridge GM (2022) Caring for patients with cognitive dysfunction, fluctuations and dementia caused by Parkinson's disease. *Prog Brain Res* **269**, 407-434.

[8] Zhang Q, Aldridge GM, Narayanan NS, Anderson SW, Uc EY (2020) Approach to cognitive impairment in Parkinson's disease. *Neurotherapeutics* **17**, 1495-1510.

[9] Kim S, Kwon S-H, Kam T-I, Panicker N, Karuppagounder SS, Lee S, Lee JH, Kim WR, Kook M, Foss CA, Shen C, Lee H, Kulkarni S, Pasricha PJ, Lee G, Pomper MG, Dawson VL, Dawson TM, Ko HS (2019) Transneuronalpropagation of pathologic α-synuclein from the gut to the brain models Parkinson's disease. *Neuron* **103**, 627-641.e7.

[10] Luk KC, Song C, O'Brien P, Stieber A, Branch JR, Brunden KR, Trojanowski JQ, Lee VM-Y (2009) Exogenous α-synuclein fibrils seed the formation of Lewy body-like intracellular inclusions in cultured cells. *Proc Natl Acad Sci USA* **106**, 20051-20056.

[11] Luk KC, Kehm V, Carroll J, Zhang B, O'Brien P, Trojanowski JQ, Lee VM-Y (2012) Pathological α-synuclein transmission initiates Parkinson-like neurodegeneration in nontransgenic mice. *Science* **338**, 949-953.

[12] Volpicelli-Daley LA, Luk KC, Patel TP, Tanik SA, Riddle DM, Stieber A, Meaney DF, Trojanowski JQ, Lee VM-Y (2011) Exogenous α-synuclein fibrils induce Lewy body pathology leading to synaptic dysfunction and neuron death. *Neuron* **72**, 57-71.

[13] Milanese C, Cerri S, Ulusoy A, Gornati SV, Plat A, Gabriels S, Blandini F, Di Monte DA, Hoeijmakers JH, Mastroberardino PG (2018) Activation of the DNA damage response *in vivo* in synucleinopathy models of Parkinson's disease. *Cell Death Dis* **9**, 818.

[14] Ayers JI, Riffe CJ, Sorrentino ZA, Diamond J, Fagerli E, Brooks M, Galaleldeen A, Hart PJ, Giasson BI (2018) Localized induction of wild-type and mutant alpha-synuclein aggregation reveals propagation along neuroanatomical tracts. *J Virol* **92**, e00586-18.

[15] Challis C, Hori A, Sampson TR, Yoo BB, Challis RC, Hamilton AM, Mazmanian SK, Volpicelli-Daley LA, Gradinaru V (2020) Gut-seeded α-synuclein fibrils promote gut dysfunction and brain pathology specifically in aged mice. *Nat Neurosci* **23**, 327-336.

[16] Henrich MT, Geibl FF, Lakshminarasimhan H, Stegmann A, Giasson BI, Mao X, Dawson VL, Dawson TM, Oertel WH, Surmeier DJ (2020) Determinants of seeding and spreading of α-synuclein pathology in the brain. *Sci Adv* **6**, eabc2487.

[17] Rahayel S, Mišić B, Zheng Y-Q, Liu Z-Q, Abdelgawad A, Abbasi N, Caputo A, Zhang B, Lo A, Kehm V, Kozak M, Yoo HS, Dagher A, Luk KC (2022) Differentially targeted seeding reveals unique pathological alpha-synuclein propagation patterns. *Brain* **145**, 1743-1756.

[18] Rey NL, Steiner JA, Maroof N, Luk KC, Madaj Z, Trojanowski JQ, Lee VM-Y, Brundin P (2016) Widespread transneuronal propagation of α-synucleinopathy triggered in olfactory bulb mimics prodromal Parkinson's disease. *J Exp Med* **213**, 1759-1778.

[19] Rey NL, George S, Steiner JA, Madaj Z, Luk KC, Trojanowski JQ, Lee VM-Y, Brundin P (2018) Spread of

aggregates after olfactory bulb injection of α-synuclein fibrils is associated with early neuronal loss and is reduced long term. *Acta Neuropathol* **135**, 65-83.

[20] Uemura N, Ueda J, Yoshihara T, Ikuno M, Uemura MT, Yamakado H, Asano M, Trojanowski JQ, Takahashi R (2021)α-synuclein spread from olfactory bulb causes hyposmia, anxiety, and memory loss inBAC-*SNCA*mice. *Mov Disord* **36**, 2036-2047.

[21] Espa E, Clemensson EKH, Luk KC, Heuer A, Björklund T, Cenci MA (2019) Seeding of protein aggregation causes cognitive impairment in rat model of cortical synucleinopathy. *Mov Disord* **34**, 1699-1710.

[22] Peeraer E, Bottelbergs A, Van Kolen K, Stancu I-C, Vasconcelos B, Mahieu M, Duytschaever H, Ver Donck L, Torremans A, Sluydts E, Van Acker N, Kemp JA, Mercken M, Brunden KR, Trojanowski JQ, Dewachter I, Lee VMY, Moechars D (2015) Intracerebral injection of preformed synthetic tau fibrils initiates widespread tauopathy and neuronal loss in the brains of tau transgenic mice. *Neurobiol Dis* **73**, 83-95.

[23] Zhang Q, Abdelmotilib H, Larson T, Keomanivong C, Conlon M, Aldridge GM, Narayanan NS (2021) Cortical alpha-synuclein preformed fibrils do not affect interval timing in mice. *Neurosci Lett* **765**, 136273.

[24] Abdelmotilib H, Maltbie T, Delic V, Liu Z, Hu X, Fraser KB, Moehle MS, Stoyka L, Anabtawi N, Krendelchtchikova V, Volpicelli-Daley LA, West A (2017) α-Synuclein fibril-induced inclusion spread in rats and mice correlates with dopaminergic neurodegeneration. *Neurobiol Dis* **105**, 84-98.

[25] Balci F, Papachristos EB, Gallistel CR, Brunner D, Gibson J, Shumyatsky GP (2008) Interval timing in genetically modified mice: A simple paradigm. *Genes Brain Behav***7**, 373-384.

[26] Bruce RA, Weber MA, Volkman RA, Oya M, Emmons EB, Kim Y, Narayanan NS (2021) Experience-related enhancements in striatal temporal encoding. *Eur J Neurosci* **54**, 5063-5074.

[27] Larson T, Khandelwal V, Weber MA, Leidinger MR, Meyerholz DK, Narayanan NS, Zhang Q (2022) Mice expressing P301S mutant human tau have deficits in interval timing. *Behav Brain Res* **432**, 113967.

[28] Weber MA, Sivakumar K, Tabakovic EE, Oya M, Aldridge GM, Zhang Q, Simmering JE, Narayanan NS (2023) Glycolysis-enhancing α1-adrenergic antagonists modify cognitive symptoms related to Parkinson's disease. *NPJ-Parkinsons Dis* **9**, 32.

[29] Gawel K, Gibula E, Marszalek-Grabska M, Filarowska J, Kotlinska JH (2019) Assessment of spatial learning and memory in the Barnes maze task in rodents—methodological consideration. *NaunynSchmiedebergs Arch Pharmacol* **392**, 1-18.

[30] O'Leary TP, Brown RE (2013) Optimization of apparatus design and behavioral measures for the assessment of visuo-spatial learning and memory of mice on the Barnes maze. *Learn Mem* **20**, 85-96.

[31] Kraeuter A-K, Guest PC, Sarnyai Z (2019) The open field test for measuring locomotor activity and anxiety-like behavior. In *Pre-Clinical Models*, Guest PC, ed. Springer New York, New York, pp. 99-103.

[32] Tatem KS, Quinn JL, Phadke A, Yu Q, Gordish-Dressman H, Nagaraju K (2014) Behavioral and locomotor measurements using an open field activity monitoring system for skeletal muscle diseases. *JoVE*, 51785.

[33] Fisher SP, Godinho SIH, Pothecary CA, Hankins MW, Foster RG, Peirson SN (2012) Rapid assessment of sleep-wake behavior in mice. *J Biol Rhythms* **27**, 48-58.

[34] Neely CLC, Pedemonte KA, Boggs KN, Flinn JM (2019) Nest building behavior as an early indicator of behavioral deficits in mice. *JoVE*, 60139.

[35] Gaskill BN, Karas AZ, Garner JP, Pritchett-Corning KR (2013) Nest building as an indicator of health and welfare in laboratory mice. *JoVE*, 51012.

[36] Franklin KBJ, Paxinos G (2008) *The mouse brain in stereotaxic coordinates*, Elsevier Academic Press, Amsterdam Heidelberg.

[37] Rey NL, Bousset L, George S, Madaj Z, Meyerdirk L, Schulz E, Steiner JA, Melki R, Brundin P (2019) α-Synuclein conformational strains spread, seed and target neuronal cells differentially after injection into the olfactory bulb. *Acta NeuropatholCommun***7**, 221.

[38] Gumusoglu SB, Chilukuri ASS, Hing BWQ, Scroggins SM, Kundu S, Sandgren JA, Santillan MK, Santillan DA, Grobe JL, Stevens HE (2021) Altered offspring neurodevelopment in an arginine vasopressin preeclampsia model. *Transl Psychiatry* **11**, 79.

[39] Gumusoglu SB, Hing BWQ, Chilukuri ASS, Dewitt JJ, Scroggins SM, Stevens HE (2020) Chronic maternal interleukin-17 and autism-related cortical gene expression, neurobiology, and behavior. *Neuropsychopharmacol* **45**, 1008-1017.

[40] Gumusoglu SB, Fine RS, Murray SJ, Bittle JL, Stevens HE (2017) The role of IL-6 in neurodevelopment after prenatal stress. *Brain Behav Immunity* **65**, 274-283.

[41] Stoyka LE, Arrant AE, Thrasher DR, Russell DL, Freire J, Mahoney CL, Narayanan A, Dib AG, Standaert DG, Volpicelli-Daley LA (2020) Behavioral defects associated with amygdala and cortical dysfunction in mice with seeded α-synuclein inclusions. *Neurobiol Dis* **134**, 104708.

[42] Peterson DA (1999) Quantitative histology using confocal microscopy: Implementation of unbiased stereology procedures. *Methods* **18**, 493-507.

[43] Gundersen HJG, Jensen EBV, Kieu K, Nielsen J (1999) The efficiency of systematic sampling in stereology - reconsidered. *J Microsc* **193**, 199-211.

[44] Anastasiades PG, Carter AG (2021) Circuit organization of the rodent medial prefrontal cortex. *Trends Neurosci* **44**, 550-563.

[45] Souza R, Bueno D, Lima LB, Muchon MJ, Gonçalves L, Donato J, Shammah-Lagnado SJ, Metzger M (2022) Top-down projections of the prefrontal cortex to the ventral tegmental area, laterodorsal tegmental nucleus, and median raphe nucleus. *Brain Struct Funct* **227**, 2465-2487.

[46] Gabbott PLA, Warner TA, Jays PRL, Salway P, Busby SJ (2005) Prefrontal cortex in the rat: Projections to subcortical autonomic, motor, and limbic centers. *J Comp Neurol* **492**, 145-177.

[47] Burwell RD, Amaral DG (1998) Cortical afferents of the perirhinal, postrhinal, and entorhinal cortices of the rat. *J Comp Neurol* **398**, 179-205.

[48] Sun F, Salinas AG, Filser S, Blumenstock S, Medina-Luque J, Herms J, Sgobio C (2022) Impact of α-synuclein spreading on the nigrostriatal dopaminergic pathway depends on the onset of the pathology. *Brain Pathol* **32**, e13036.

[49] Kim Y-C, Han S-W, Alberico SL, Ruggiero RN, De Corte B, Chen K-H, Narayanan NS (2017) Optogenetic stimulation of frontal D1 neurons compensates for impaired temporal

control of action in dopamine-depleted mice. *CurrBiol* **27**, 39-47.

[50] Malapani C, Rakitin B, Levy R, Meck WH, Deweer B, Dubois B, Gibbon J (1998) Coupled temporal memories in Parkinson's disease: A dopamine-related dysfunction. *J CognNeurosci* **10**, 316-331.

[51] Pastor MA, Artieda J, Jahanshahi M, Obeso JA (1992) Time estimation and reproduction is abnormal in Parkinson's disease. *Brain* **115**, 211-225.

[52] Singh A, Cole RC, Espinoza AI, Evans A, Cao S, Cavanagh JF, Narayanan NS (2021) Timing variability and midfrontal ∼4 Hz rhythms correlate with cognition in Parkinson's disease. *NPJParkinsons Dis***7**, 14.

[53] Emmons EB, De Corte BJ, Kim Y, Parker KL, Matell MS, Narayanan NS (2017) Rodent medial frontal control of temporal processing in the dorsomedial striatum. *J Neurosci* **37**, 8718-8733.

[54] Narayanan NS, Land BB, Solder JE, Deisseroth K, DiLeone RJ (2012) Prefrontal D1 dopamine signaling is required for temporal control. *Proc Natl Acad Sci USA* **109**, 20726-20731.

[55] Luk KC, Covell DJ, Kehm VM, Zhang B, Song IY, Byrne MD, Pitkin RM, Decker SC, Trojanowski JQ, Lee VM-Y (2016) Molecular and biological compatibility with host alpha-synuclein influences fibril pathogenicity. *Cell Rep* **16**, 3373-3387.

[56] Adhikari A, Lerner TN, Finkelstein J, Pak S, Jennings JH, Davidson TJ, Ferenczi E, Gunaydin LA, Mirzabekov JJ, Ye L, Kim S-Y, Lei A, Deisseroth K (2015) Basomedial amygdala mediates top-down control of anxiety and fear. *Nature* **527**, 179-185.

[57] Vidal-Gonzalez I, Vidal-Gonzalez B, Rauch SL, Quirk GJ (2006) Microstimulation reveals opposing influences of prelimbic and infralimbic cortex on the expression of conditioned fear. *Learn Mem* **13**, 728-733.

[58] Hamilton DA, Brigman JL (2015) Behavioral flexibility in rats and mice: Contributions of distinct frontocortical regions. *Genes Brain Behav* **14**, 4-21.

[59] Manfredsson FP, Luk KC, Benskey MJ, Gezer A, Garcia J, Kuhn NC, Sandoval IM, Patterson JR, O'Mara A, Yonkers R, Kordower JH (2018) Induction of alpha-synuclein pathology in the enteric nervous system of the rat and non-human primate results in gastrointestinal dysmotility and transient CNS pathology. *Neurobiol Dis* **112**, 106-118.

[60] Uemura N, Uemura MT, Lo A, Bassil F, Zhang B, Luk KC, Lee VM-Y, Takahashi R, Trojanowski JQ (2019) Slow progressive accumulation of oligodendroglial alpha-synuclein (α-Syn) pathology in synthetic α-Syn fibril-induced mouse models of synucleinopathy. *J Neuropathol Exp Neurol* **78**, 877-890.

[61] Uemura N, Marotta N, Ara J, Meymand E, Zhang B, Kameda H, Koike M, Luk K, Trojanowski J, Lee V (2023) Distinct biological activity of Lewy body α-Synuclein strain in mice. *Res Sq*, rs.3.rs-2579805.

[62] Beas BS, McQuail JA, Bañuelos C, Setlow B, Bizon JL (2017) Prefrontal cortical GABAergic signaling and impaired behavioral flexibility in aged F344 rats. *Neuroscience* **345**, 274-286.

[63] Gür E, Duyan YA, Arkan S, Karson A, Balcı F (2020) Interval timing deficits and their neurobiological correlates in aging mice. *Neurobiol Aging* **90**, 33-42.

[64] Stutt HR, Weber MA, Cole RC, Bova AS, Ding X, McMurrin MS, Narayanan NS (2023) Sex similarities and dopaminergic differences in interval timing. *bioRxiv,* doi: 10.1101/2023.05.05.539584.

[65] Savica R, Grossardt BR, Bower JH, Boeve BF, Ahlskog JE, Rocca WA (2013) Incidence of dementia with Lewy bodies and Parkinson disease dementia. *JAMA Neurol* **70**, 1396.

[66] Van Den Eeden SK (2003) Incidence of Parkinson's disease: Variation by age, gender, and race/ethnicity. *Am J Epidemiol* **157**, 1015-1022.

[67] Wooten GF (2004) Are men at greater risk for Parkinson's disease than women? *J NeurolNeurosurg Psychiatry* **75**, 637-639.

[68] Morigaki R, Lee JH, Yoshida T, Wüthrich C, Hu D, Crittenden JR, Friedman A, Kubota Y, Graybiel AM (2020) Spatiotemporal up-regulation of mu opioid receptor 1 in striatum of mouse model of Huntington's disease differentially affecting caudal and striosomal regions. *Front Neuroanat* **14**, 608060.